This is the accepted manuscript made available via CHORUS. The article has been published as:

Soft phonon mode dynamics in Aurivillius-type structures

Deepam Maurya, Ali Charkhesht, Sanjeev K. Nayak, Fu-Chang Sun, Deepu George, Abhijit Pramanick, Min-Gyu Kang, Hyun-Cheol Song, Marshall M. Alexander, Djamila Lou, Giti A. Khodaparast, S. P. Alpay, N. Q. Vinh, and Shashank Priya

Phys. Rev. B **96**, 134114 — Published 18 October 2017

DOI: 10.1103/PhysRevB.96.134114

Soft Phonon Mode Dynamics in Aurivillius Type Structures

Deepam Maurya[1,2], Ali Charkhesht[3], Sanjeev K. Nayak[4], Fu-Chang Sun[4], Deepu George[3], Abhijit Pramanick[5], Min-Gyu Kang[1], Hyun–Cheol Song[1,6], Marshall M. Alexander[3], Djamila Lou[3], Giti A. Khodaparast[3], S. P. Alpay[4,*], N. Q. Vinh[3,*], and Shashank Priya[1,2,*]

[1]*Bio-inspired Materials and Devices Laboratory (BMDL), Center for Energy Harvesting Materials and Systems (CEHMS), Virginia Tech, Blacksburg, VA 24061 USA*

[2]*Institute for Critical Technology and Applied Science (ICTAS), Virginia Tech, Blacksburg, Virginia 24061, USA*

[3]*Department of Physics and Center of Soft Matter and Biological Physics, Virginia Tech, Blacksburg, VA 24061 USA*

[4]*Department of Materials Science & Engineering, Department of Physics, Institute of Materials Science, University of Connecticut, Storrs, CT 06269-3136, USA*

[5]*Department of Materials Science and Engineering, City University of Hong Kong, Kowloon, Hong Kong SAR*

[6]*Center for Electronic Materials, Korea Institute of Science and Technology (KIST), Seoul 02792, Republic of Korea*

e-mail address: pamir.alpay@uconn.edu, vinh@vt.edu, spriya@vt.edu

We report the dynamics of soft phonon modes and their role towards the various structural transformations in Aurivillius materials by employing terahertz frequency-domain spectroscopy, atomic pair distribution function analysis, and first-principles calculations. We have chosen the $Bi_4Ti_3O_{12}$ material as a model system and identified soft phonon modes associated with the paraelectric tetragonal to the ferroelectric monoclinic transition. Three soft phonon modes have been discovered which exhibit a strong temperature dependence. We have determined that the anharmonicity in Bi−O bonds plays a significant role in phonon softening and that Bi cations play an important role in the emergence of ferroelectricity.

PACS: 78.30.-j, 63.20.-e, 77.80.B-, 77.80.-e

I. INTRODUCTION

The knowledge of soft phonon mode properties is crucial for understanding the origin of lattice instabilities and structural phase transitions in bismuth layered ferroelectrics (Aurivillius-type structures represented as $[Bi_2O_2][A_{m-1}B_mO_{3m+1}]$, where m = 3, A = Bi, and B=Ti, for $Bi_4Ti_3O_{12}$). Typically, ferroelectric-paraelectric phase transitions in these materials occur with the heavily damped phonons in the terahertz (THz) frequencies [1,2]. Additionally, there could be subtle structural distortions below Curie temperature (T_c), which are often difficult to correlate with phonon dynamics. Since structural changes drive many material properties, a fundamental understanding of dynamics of these phonon modes is critical for designing high performance ferroelectric materials and devices [3]. The number of phonon modes are defined by the nature of changes in the symmetry during the transitions. The phase transitions involving more than one soft phonon modes [4] and corresponding order parameters, may induce structural transformations at temperatures below T_c. However, the condensation of more than one phonon modes at a single transition is quite unusual [5]. Using a sensitive and high resolution THz frequency-domain spectroscopy, we have experimentally discovered the so far elusive three phonon modes in $Bi_4Ti_3O_{12}$ (BiT) system. These phonon modes, not reported earlier, are expected to have important implications towards the symmetry breaking from the high temperature tetragonal to the low temperature monoclinic phase as well as structural transformations below Curie temperature (T_c).

Here, we have employed the BiT as a model system to understand phonon modes related to phase transitions in Aurivillius materials [6]. The ferroelectric members of this family have potential for high temperature sensors and fatigue-free ferroelectric memory devices etc. [7,8]. The structure of BiT consists of perovskite-like block $(Bi_2Ti_3O_{10})^{2-}$ interleaved with fluorite like $(Bi_2O_2)^{2+}$ layers perpendicular to pseudo-tetragonal c-axis [9,10]. In terms of phase transformation characteristics, BiT undergoes a transition from the high temperature tetragonal paraelectric phase to a lower temperature monoclinic polar phase [11]. This phase transition involves displacement of Bi atoms together with rotation of the TiO_6 octahedra. [12]

Much effort has been devoted to understand structural changes with respect to temperature in Aurivillius ferroelectric materials [5,13]. The low temperature ferroelectric monoclinic phase of BiT requires condensation of at least three different symmetry breaking modes, which have hitherto not been observed experimentally [5]. An observation of the temperature dependence of the lowest frequency polar phonon mode (denoted as a soft phonon mode), using Raman scattering is not very convincing, because the intensity of the soft phonon mode decreases

* Corresponding authors: pamir.alpay@uconn.edu, vinh@vt.edu, spriya@vt.edu

rapidly with increasing temperature [4]. Prior studies have investigated the dynamics of the ferroelectric transition in Bi-layered ferroelectric materials using THz time-domain spectroscopy [4,14], where only one optical soft mode was observed in the ferroelectric phase of the BiT material [4], which was underdamped above the phase transition temperature (T_c) due to the change of selection rules in the paraelectric phase. However, in present work, using a high resolution and large dynamic range THz frequency-domain spectroscopy [15], we have observed multiple optical modes which could explain the various structural transformations in BiT and BiT-like layered materials. We further employed atomic pair distribution function (PDF) analysis and the first-principles calculations to provide the fundamental understanding of phonon dynamics in layered ferroelectrics.

II. EXPERIMENTAL DETAILS

The THz experiments were performed on (00l) textured (oriented) BiT ceramics (see Appendix A1–A5). For PDF analysis, high resolution powder x-ray diffraction data were recorded using beamline 11-BM at Argonne National Laboratory. Transmission electron microscopy (TEM) images were performed using the FEI Titan 300 electron microscope. The THz frequency-domain spectrometer consists of a commercial Vector Network Analyzer from Agilent, the N5225A PNA which covered the frequency range from 10 MHz to 50 GHz, and THz frequency extenders as well as matched harmonic detectors developed by Virginia Diodes, Inc. with frequency range from 60 GHz to 1.12 THz. The dynamic range of the instrument reaches 10^{13} with a spectral resolution of less than 100 Hz. The details of the THz measurement are described in Appendix A3.

III. RESULTS AND DISCUSSION

Figure 1a shows a bright field cross-section TEM image of textured BiT samples. The cross-section morphology indicates that the plate-type BiT grains are stacked along the thickness of the sample confirming the textured microstructure of the BiT material. From these images the size of the plate-type grains is in the range of 5−15 μm (see Appendix A2 on morphology analysis). The thickness of these plate type grains was found to be in the range of 200–500 nm (Fig. 1a). The stacking of the pseudo-perovskite and $(Bi_2O_2)^{2+}$ layers was clearly observed in the HR-TEM lattice fringes from [100] zone axis, as shown in Fig. 1b. The upper inset in Fig. 1b shows the FFT pattern indicating [100] zone axis, whereas, the lower inset indicates a TEM image with low magnification, revealing layered structure. Due to the two-fold in-plane symmetry, the distinctive stacking of the pseudo-perovskite and $(Bi_2O_2)^{2+}$ layers was not observed from [001] zone axis.(Appendix A2) The schematic of BiT layered structure at low temperature phase is provided in Fig. 1c.

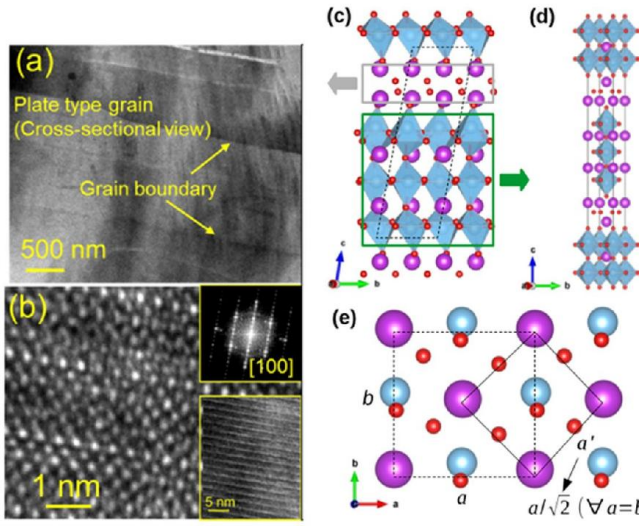

FIG. 1. (Color online) (a) Bright field cross-section TEM image of plate type grains in BiT indicates that the thickness is in the range of 200–500 nm. (b) The HR-TEM lattice fringe images of BiT ceramics observed from zone axis [100] indicate the stacking of the pseudo-perovskite and $(Bi_2O_2)^{2+}$ layers. The lower inset of (b) shows the corresponding low magnification image. Note that images of Bi_2O_2 layers in the HR-TEM image are collected with the electron beam parallel to the [100] zone axis. The upper inset of (b) depicts the corresponding FFT patterns indicating [100] zone axis. Low and high temperature phases of the BiT structures are shown in (c) and (d), respectively. Bi is denoted by large (purple) spheres, O by small (red) spheres. Ti ions stay at the center of the octahedron surrounded by six O atoms. (e) A suggested transformation path from monoclinic to tetragonal symmetries. This transition is associated with the opposite movement of the fluorite- and perovskite-like layers, indicated by arrows (gray and

The high dynamic range and high resolution of our THz frequency-domain spectroscopy allows us to observe the lowest-frequency polar phonon modes or soft phonon modes. The refractive index, $n(\nu)$, and absorption coefficient, $\alpha(\nu)$, of BiT samples have been determined through THz measurements, as shown in Figs 2a and 2b, respectively for several temperatures from room temperature to near T_c at 600ºC. The frequency-dependent complex dielectric response, $\varepsilon^*(\nu) = \varepsilon'(\nu) - i\varepsilon''(\nu)$, is related to the complex refractive index, $n^*(\nu) = n(\nu) - i\kappa(\nu)$, through the relations:

$$\epsilon'_{sol}(\nu) = n^2(\nu) - \kappa^2(\nu) = n^2(\nu) - (c\alpha(\nu)/4\pi\nu)^2$$
$$\epsilon''_{sol}(\nu) = 2n(\nu)\cdot\kappa(\nu) = 2n(\nu)c\alpha(\nu)/4\pi\nu \quad (1)$$

where ν is the frequency of the THz radiation. The real part, $n(\nu)$, is the refractive index and the imaginary part, $\kappa(\nu)$, is the extinction coefficient and indicates the attenuation when the radiation propagates through the material. The extinction coefficient, $\kappa(\nu)$, is related to the absorption coefficient through a relation: $\alpha(\nu) = \frac{4\pi\cdot\nu\kappa(\nu)}{c}$, where c is the speed of light.

Accounting these relationships, we have obtained the complex dielectric response of the BiT sample including the dielectric loss, $\varepsilon''(\nu)$ and permittivity $\varepsilon'(\nu)$ as a function of THz frequency at various temperatures up to T_c of the material (Figs 2c and 2d), respectively. Unlike the previous reports where only one mode was reported at 0.83 THz [4,7], we have observed three phonon modes at 0.68 THz (22.68 cm^{-1}), 0.86 THz (28.69 cm^{-1}) and 0.96 THz (32.02 cm^{-1}) at room temperature for the 30 μm BiT sample. The observations were reproducible (3 different samples) and the temperature cycling did not noticeably affect the observed phonon modes. A strong temperature dependence of these phonon modes and the corresponding phonon mode frequencies decreasing toward zero near the T_c, appear to suggest their soft mode behavior. The theoretical calculations further confirm soft nature of the phonon modes. Upon heating, in addition to mode shifting, the full width at half maximum (FWHM) of the absorption peak also increases with temperature.

To gain better insight into the damping process of the three soft phonon modes, we have fitted the complex dielectric response obtained from our THz frequency-domain spectroscopy at various temperatures. For this, we have employed a function containing a sum of three damped Lorentz oscillators describing the optical phonons of the ferroelectric materials [16]:

$$\varepsilon^*(\nu) = \varepsilon_\infty + \sum_{j=1}^{3} \frac{A_j/(2\pi)^2}{\nu_j^2 - \nu^2 + i\nu(\gamma_j)} \qquad (2)$$

where $A_j/(2\pi)^2$, ν_j, and γ_j are, respectively, the spectral amplitude of the j damped resonances, its frequency, and its damping coefficient, ε_∞ describes contributions to the dielectric function from modes at frequencies much greater than our experimental range. The parameters of three soft-phonon modes as function of sample temperature are summarized in Figs 2*e*, 2*f*, and 2*g*. The resonant frequencies of the three soft phonon modes (ν_1, ν_2, and ν_3) decreases with increasing sample temperature. The damping of these modes increases with the sample temperature. Specifically, while the damping and FWHM values for the ν_1 phonon mode slightly change with the sample temperature, these parameters for the ν_2, and ν_3 modes exhibit a strong increase with increasing temperature, which suggests a finite

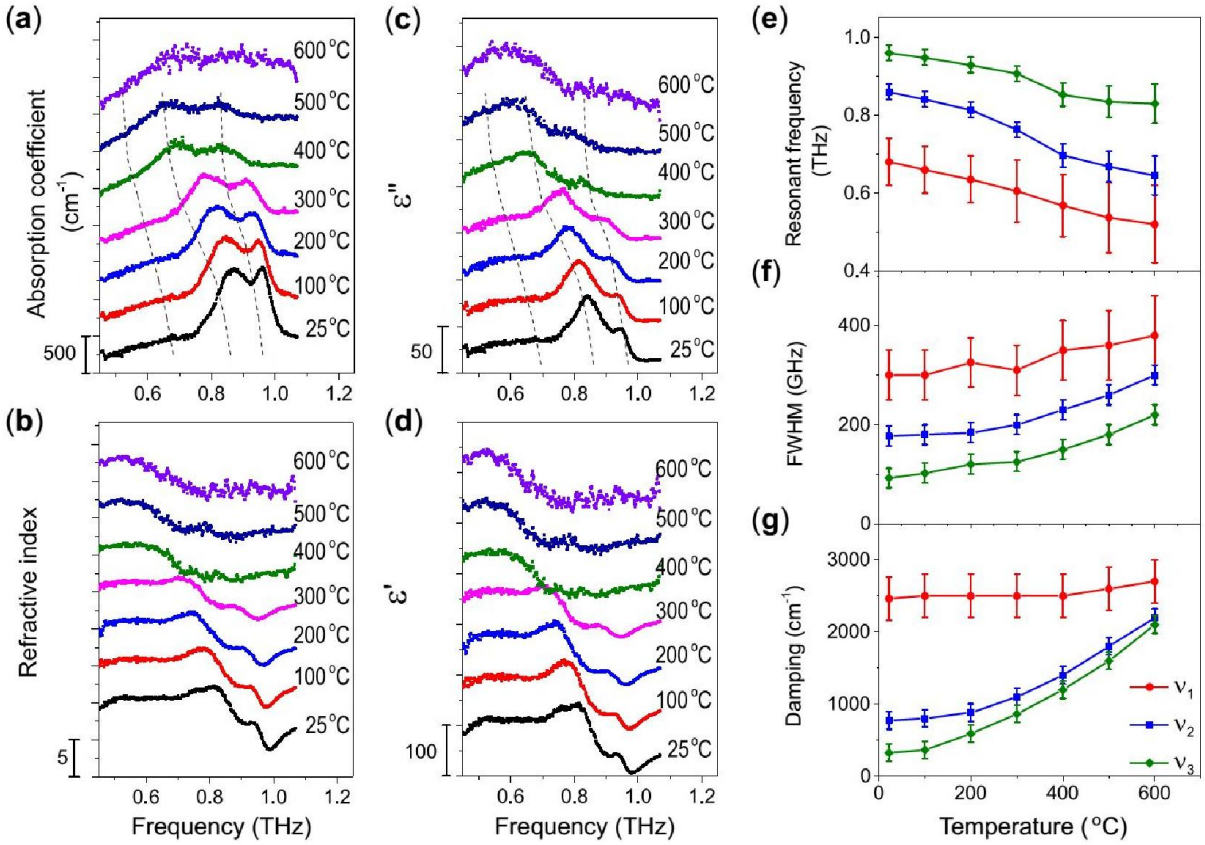

FIG. 2. (Color online) The terahertz (a) absorption and (b) refractive index of the *c*-oriented textured polycrystalline BiT ceramic material recorded at various temperatures. Complex THz dielectric response including (c) the dielectric loss and (d) the permittivity at different temperatures calculated from their absorption and refractive index. Employing the three-damped oscillator model, we extracted values for (e) soft optical phonon frequencies ν_1, ν_2, and ν_3, (f) FWHM and (g) phonon damping factors γ_1, γ_2, γ_3. The curves are shifted for clarity in panels (a-d) and the dash lines are guide to eye.

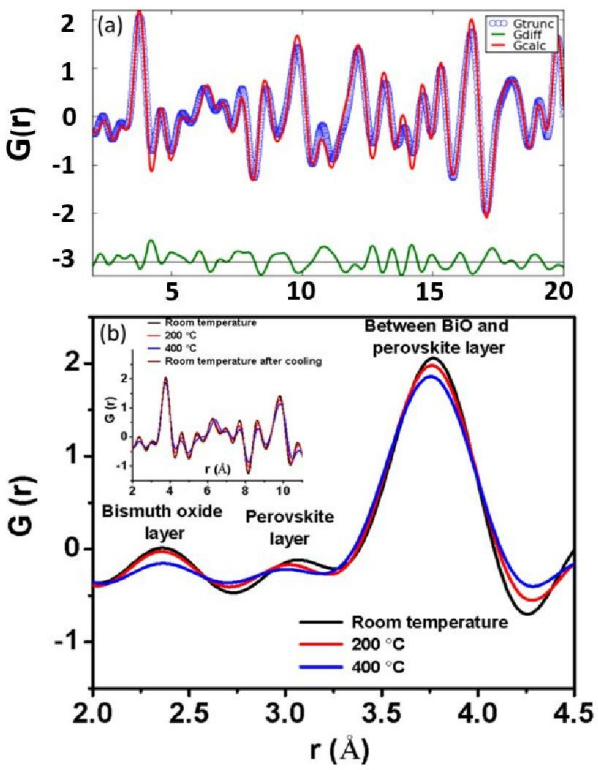

FIG. 3. (Color online) (a) The fit obtained using PDFGUI for B2cb structure in BiT. (b) Peaks indicate the closest neighbor Bi–O bonds. The Bi–O bonds show significant disordered structure at higher temperatures for both bismuth oxide and the perovskite layers. The inset of Fig. 3(b) shows the pair distribution functions, G(r), measured under different conditions, providing a relation between the dynamics of Bi ions with phonon dynamics. The calculated pattern for the B2cb structure is shown with dotted

coupling between these modes. The results are indication of the soft nature of these phonon modes.

The pronounced softening of the ν_2 and ν_3 modes with increasing temperature can be understood as a result of impending ferroelectric-to-paraelectric phase transition as the sample temperature approaches $T_c \sim 690$ °C by combining the THz spectroscopy with the atomic PDF measurements and the first-principle calculation. The anomalies below T_c could be observed from the THz spectra, as shown in Fig. 2. A discontinuity in the temperature dependence and a sharp increase in FWHM for all these modes occur at T > 300 °C. The damping of these phonon modes increase significantly when the sample temperature reaches near to T_c. In order to understand the possible structural distortions, which might explain anomalies observed below T_c, we have performed the atomic PDF measurements. The PDF measurements obtained from a total scattering XRD pattern via a Fourier transform provides us an approach to study the local structure of materials. Because the total scattering pattern is composed of Bragg as well as diffuse scattering contributions, the information contains local, medium range and long range structure information. The high energy XRD results were corrected for the sample absorption, background, Compton scattering, and incident flux. The intensities were normalized and reduced to the structure factor S(Q) (where Q is the diffraction wave vector), which was Fourier transformed to the corresponding PDFs using PDFgetX [17], G(r) (see Appendix A4). The G(r) gives the probability of finding a pair of atoms at a distance r [18]:

$$G(r) = \frac{2}{\pi}\int_0^\infty Q[S(Q) - 1]\sin(Qr)\,dQ \qquad (3)$$

Having the experimental PDF, one usually wants to determine local structural changes. The PDF results were fitted with B2cb structure having lattice parameters a = 5.448 Å, b = 5.411 Å, c = 32.83 Å, as shown in Fig. 3*a*. The atomic positions were same as given by Rae et al. [19]. The peaks for the nearest neighbors are highlighted in Fig. 3*b*. The inset of Fig. 3*b* shows the experimental PDF, G(r), for the BiT at different conditions. One can clearly see the broadening of the peaks related to the bismuth oxide layer and perovskite layer at 400 °C (Fig. 3b). The broadening of these peaks indicates increasing disorder in bismuth layers. Most notably, the peak related to the perovskite layer is not just broadened, but also, became asymmetric indicating increased anharmonicity of the Bi–O bonds. We have determined that the anharmonicity of these bonds plays a significant role in shifting of the soft phonon modes, and

TABLE I. Table showing the lattice parameters of various models considered in this study. Here, a, b and c are lattice parameters (Å), α_0 (degrees) and V_0 (Å^3/unitcell) are the monoclinic lattice angle and volume for the ground state crystal structure.

	Volume	*a*	*b*	*c*	*α*	*β*	*γ*
DFT (present)	506.252	5.493	5.533	16.883	80.609	90	90
1.004 α_0	506.252	5.450	5.522	17.034	80.933	90	90
1.007 α_0	506.252	5.436	5.525	17.060	81.148	90	90
1.015 V_0	513.884	5.521	5.560	16.968	80.609	90	90
1.03 V_0	521.592	5.548	5.588	17.052	80.609	90	90
Tetragonal	492.676	3.852	3.852	33.197	90	90	90
Ref. [19]	486.652	3.85	3.85	32.832	90	90	90

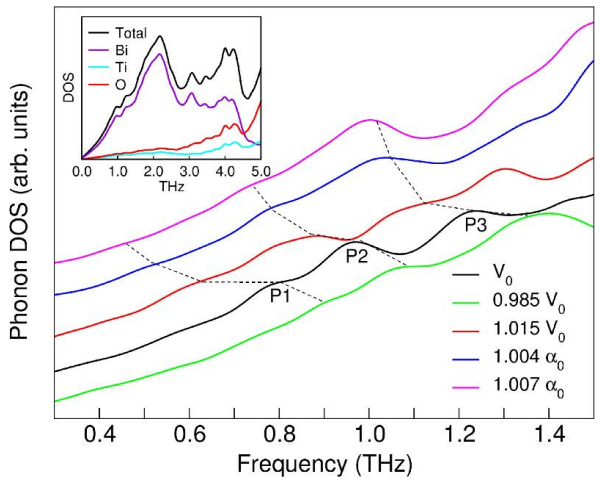

FIG. 4. (Color online) The phonon DOS for the ground state monoclinic structure (V_0) is shown as black line. The DOS for volume change -1.5% (0.985 V_0) and +1.5 (1.015 V_0) are shown as green and red lines, while that for change in lattice angle α by 0.4% (1.004 α_0) and 0.7% (1.007 α_0) are shown as blue and magenta solid lines, respectively. The peaks shift to lower frequencies in all cases due to deviation from the ground state lattice. The DOS is shifted for clarity. The dashed lines are guide to eye. The inset shows atomic contribution to the total phonon DOS, suggesting that a major contribution to phonons in the low energy range is from Bi atoms.

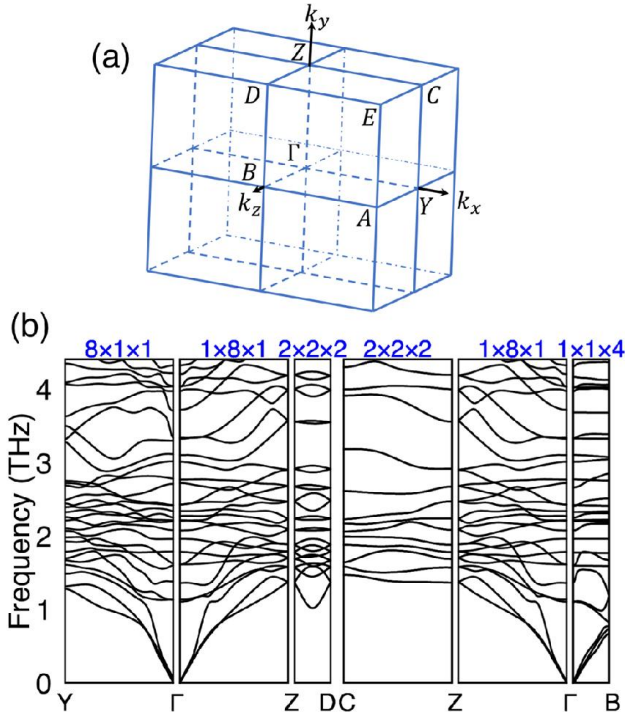

FIG. 5. (Color online) (a) Brillouin zone and (b) the phonon band structure for the monoclinic BiT lattice. The appropriate size of supercell is chosen as shown in the top panel to incorporate the commensurate q-points along the high-symmetry path.

could possibly be the origin of anomalies observed in THz spectra below T_c.

In order to obtain further insights into the experimentally observed phonon dynamics and bond anharmonicity, phonon studies were performed with first principles density functional theory (DFT) [20,21]. The generalized gradient approximation [22] was used as the exchange-correlation functional together with the projector-augmented wave method [23] as implemented in the Vienna *Ab initio* Simulation Package (VASP) [24-26]. The primitive cell dimensions for the monoclinic BiT (Table I) were found to be in good agreement with experimental reports [27] and other first-principles computations [28,29]. Phonon calculations were performed by the linear response method [30] and the frozen phonon method together with Phonopy [31]. Combination of DFT with frozen phonon method provides the platform to analyze lattice dynamics in quasi harmonic approximation with the inter-atomic forces calculated from the state-of-the-art electronic structure methods.

The phonon density of states (DOS) is shown as black solid line in Fig. 4. We identified three peaks P1, P2 and P3 in the range 0.6–1.5 THz. The phonon band structure shown in Fig. 5 indicated that P2 could be matched to two phonon modes at the Γ point which were almost degenerate and P3 is the next optical mode. The phonon band diagram was established by appropriately expanding the size of the supercell along *a*, *b* and *c* lattice vectors to account for all the commensurate *k*-points along *x*- (Γ-Y), *y*- (Γ-Z), and *z*-axes (Γ-B) of the Brillouin zone. To determine the complete band diagram, supercell of size up to 8×8×4 unit cells, consisting of 9728 atoms, is required which is not computational feasible. The eigenvalues of three low energy phonons, obtained from density functional perturbation theory (DFPT), using 2×2×1 supercell, were found to be 1.11 THz, 1.13 THz and 1.26 THz. These modes were IR active and had symmetries A", A', and A' (verified with the Quantum Espresso code). In order to observe the effect of the volume change, we computed the phonon DOS with a volume change of +1.5 % V_0 and –1.5 % V_0 shown as red and green lines in Fig. 4, respectively. We also explored the effect of octahedral tilting on the phonon DOS by increasing the monoclinic angle α_0 by 0.4% and 0.7%, as shown in Fig. 4 in blue and magenta lines, respectively. Please note that the DOS of the models are shifted in *y*-axis to compare the plots. The *y*-shift does not have a physical meaning. The crystal structure parameters for various models used in the study is tabulated in Table I. These results suggested that the phonon peaks were shifted to lower frequencies for the models deviating from the ground state monoclinic structure. The peak P2 appeared to split the constituting phonon modes by about 0.2 THz when the volume was increased. On reduction of the volume to 0.985 V_0, the phonons were found to exhibit hardening behavior. Thermodynamic analysis from Phonopy suggests the volume change is positive up to certain temperature and then start decreasing with increasing

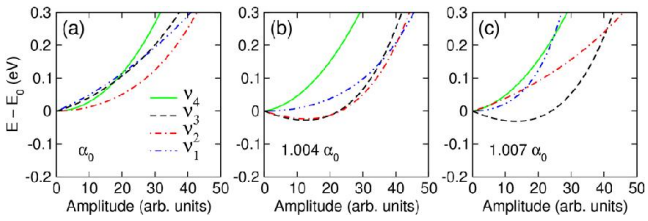

FIG. 6. (Color online) Total energy as a function of amplitude for the lowest four phonon modes for (a) perfect monoclinic structure, (b) monoclinic lattice with $\alpha = 1.004\ \alpha_0$ and (c) monoclinic lattice with $\alpha = 1.007\ \alpha_0$, respectively. The lowering in energy as a function of amplitude is a signature of soft phonon mode.

temperature (see Appendix A6). This is in line with the larger crystallographic volume of the ferroelectric monoclinic phase as compared to the paraelectric tetragonal phase of BiT as the monoclinic phase of BiT has larger volume (252.13 Å^3/unitcell) than that of the tetragonal phase (246.34 Å^3/unitcell) of BiT [32]. In order to study the soft phonon characteristics, the modes obtained for the lowest four phonon energies from DFPT calculations have been subject to variation of amplitude and the total energy of the supercells calculated using VASP as shown in Fig. 6. The models with pure monoclinic lattice (α_0), and lattice with $\alpha = 1.004\ \alpha_0$ and $\alpha = 1.007\ \alpha_0$ were chosen as these models were adapting from monoclinic towards the tetragonal structure. The lowering in energy as a function of amplitude is found for two modes for $\alpha = 1.004\ \alpha_0$. With increase α to $1.007\ \alpha_0$ one of the two modes recover, while the other undergoes further lowering in energy. The minima in these curves are 27.4 meV and 31.0 meV for $1.004\ \alpha_0$ and $1.007\ \alpha_0$ models, respectively. The lowering in energy as a function of amplitude is a signature of soft phonon mode. These results indicated that atomic rearrangement accommodating the changes in the unit cell could lead to anharmonicity in the interatomic bonds, as observed in the PDF analysis of Fig. 3.

The phonons at P2 and P3 of Fig. 4 show vibration of ions in the perovskite- and fluorite-blocks. (See Supplemental Material for animated gif files of the phonon modes [33]) The correlated motion of atoms within each block, which are out-of-phase among each other, is shown in the gray and green regions in Fig. 1c. The out-of-phase oscillations of the lattice blocks could potentially lead to the deviation from the monoclinic towards tetragonal phase (Fig. 1d). The structural change could be described using the lattice parameter transformation $a < b \rightarrow a' = b'$, such that the lattice parameter of the tetragonal phase is $a'\ (=b') = a/\sqrt{2}$ (Fig. 1*e*). This mechanism is consistent with the theoretical findings of Ref. [3], where it is suggested that two unstable E_u modes in BiT, one involving the motion of fluorite layers in a direction relative to the perovskite $(TiO_6)^{8-}$ blocks and the second mode involving the motion of the Bi ions in the perovskite A site with respect to the perovskite blocks, are responsible for the phase change. The atomic displacements in the fluorite layers are found to be larger than in the perovskite layers. Thus, we underline that the chemical nature of large cation in the fluorite layers in the Aurivillius family and similar layered oxides is crucial for structural transformations. We note, however, that the theoretical tools used here could have certain limitations when applied to more complicated crystal structures. Firstly, the quasi-harmonic approximation is not appropriate for larger scale volume and/or angular variations. In addition, this approach may not be employed to accurately determine phase transformation temperatures in strongly correlated systems. Future improvements on the current theoretical foundations will, therefore, be necessary to describe more complex systems.

IV. CONCLUSIONS

In summary, we have probed dynamics of soft phonon modes and its role in the structural transformations on (00l) oriented $Bi_4Ti_3O_{12}$ using the THz frequency-domain spectroscopy. The results from the THz frequency-domain spectroscopy have revealed three low frequency soft phonon modes, which have been supported from first-principles study and the atomic pair distribution function analysis. The anharmonicity of the Bi−O bonds plays a leading role in these low frequency phonon modes with majority of contribution to the phonon density of states comes from the Bi atoms. The fundamental understanding about various factors affecting phonon dynamics and structural changes described here provides useful information in designing tailored phase transition and functionality (e.g. ferroelectric and thermal properties) of layered-structure ferroelectric materials.

ACKNOWLEDGEMENTS

This work was supported by the AFOSR through grant FA9550-14-1-0376. The terahertz-dielectric study was supported by the Institute of Critical Technology and Applied Sciences (ICTAS) at Virginia Tech. MGK and HCS acknowledge financial support through the Department of Energy program (DE-FG02-06ER46290). The computational resources from the Taylor L. Booth Engineering Center for Advanced Technology (BECAT) at University of Connecticut is gratefully acknowledged. One of the authors (F-C. S) would like to thank J. Skelton, University of Bath and H. Tran and K. Pitike from University of Connecticut for helpful discussions. SKN would like to acknowledge technical support from Serge M. Nakhmanson, University of Connecticut and Waheed A. Adeagbo, Martin Luther University Halle-Wittenberg. Use of the Advanced Photon Source at Argonne National Laboratory was supported by the U. S. Department of Energy, Office of Science, Office of Basic Energy Sciences, under Contract No. DE-AC02-06CH11357. AP gratefully acknowledges

funding support from CityU Start-up Grant for New Faculty (Project Number 7200514). AC and SKN contributed equally to this work. SP acknowledges the support from NSF CREST program.

APPENDIX

A1. SAMPLE PREPARATION

In order to synthesize textured $Bi_4Ti_3O_{12}$ (BiT) ceramics, we first synthesized BiT platelets using molten salt synthesis method [34]. For this, stoichiometric amount of Bi_2O_3 and TiO_2 ceramics were ball milled for 24 h under ethyl alcohol in polyethylene bottle with yttria-stabilized zirconia (YSZ) balls as milling media. This slurry was further dried in an oven at 60ºC for 6 h. The resulting powder was mixed with equal amount of salt mixture (56wt% KCl and 44wt% NaCl) and heated at 1150 ºC for 30 min. Next, this product is washed several times in deionized water to remove salt and get BiT platelets. These platelets were pressed to get cylindrical pellet and sintered at 1150 ºC for 2 h. Furthermore, during high temperature processing, all the specimens were muffled with the powder of the same composition in order to maintain the chemical composition. During pressing, the anisotropic BiT particles with large aspect ratio were aligned with the major surface perpendicular to the pressing direction, which resulted in textured BiT ceramics after sintering.

A2. TEXTURE AND MICROSTRUCTURE

Room temperature XRD-spectra were recorded by using a Philips Xpert Pro x-ray diffractometer (Almelo, The Netherlands). These XRD patterns clearly suggest formation of pure BiT phase. The change in the intensity of Bragg reflections in the XRD-spectrum of textured BiT clearly suggest high degree of texturing. The degree of orientation was determined from the XRD pattern of the textured BiT in the range of 2θ = 10 – 50º by Lotgering's method. The Lotgering factor f is defined as the fraction of area textured with required crystallographic plane using the formula[35]:

$$\text{Lotgering Factor } f_{00l} = \frac{P - P_o}{1 - P_o}, P = \frac{\Sigma I(00l)}{\Sigma I(hkl)}, P_o = \frac{\Sigma I_o(00l)}{\Sigma I_o(hkl)} \quad (4)$$

where I and I_o are intensity of the diffraction lines (*hkl)* of textured and randomly oriented specimens, respectively. The

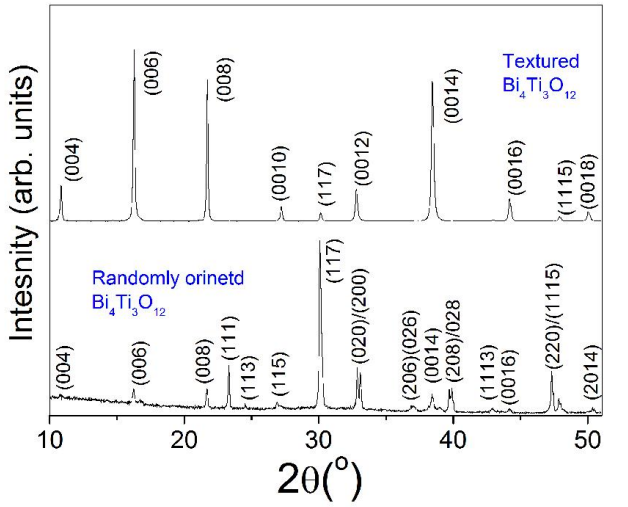

FIG. 7. (Color online) XRD spectra recorded at RT for textured and randomly oriented BiT ceramics. Please note the change in the intensity of textured BiT ceramics indicating high degree of the crystallographic orientation

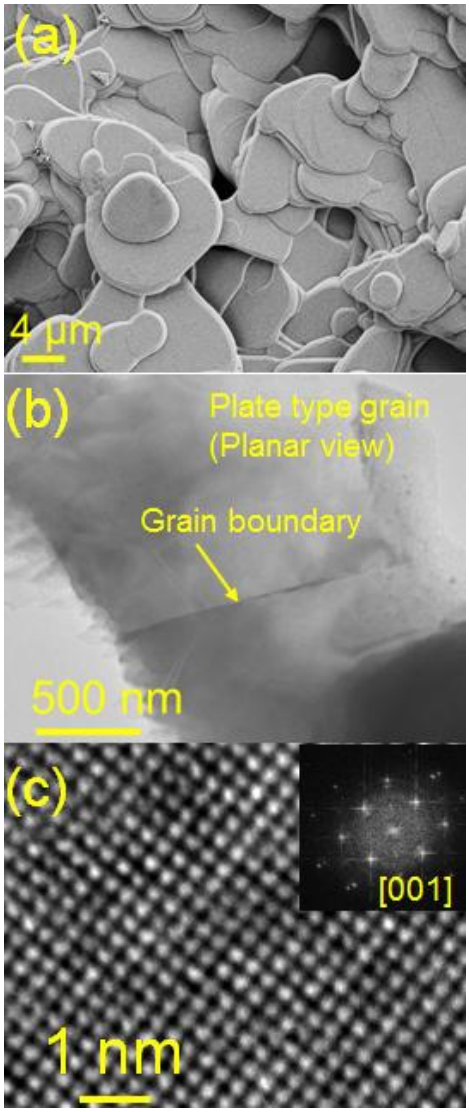

FIG. 8. (Color online) (a) SEM micrographs of <001> textured BiT from top surface. (b) Bright field TEM image of the plate type grains from the top surface. (c) The HR-TEM lattice fringe images of BiT ceramics from [001] zone axis. The inset of (c) shows FFT patterns marked with the zone axes.

degree of texturing (calculated using Lotgering factor) was found to be 96% suggesting sintered ceramics are oriented along *c*-axis.

The surface morphology of the sintered samples was observed using a LEO Zeiss 1550 (Zeiss, Munich, Germany) scanning electron microscope. In order to prepare the electron transparent TEM specimens, we used standard grinding and ion-milling method. For conducting transmission electron microscopy (TEM), we used a FEI Titan 300 microscope.

FIG. 7 shows XRD-patterns recorded at room temperature for textured BiT ceramics. The change in the intensity of various Bragg reflections compared to randomly oriented counterpart, suggests a high degree of texture along the *c*-axis. The lotgering factor f_{00l} calculated from these XRD-patterns suggested 96% texturing in <001> orientation. In order to investigate morphology of the textured BiT samples, SEM micrographs were recorded on the flat surface (Fig. 8*a*). The flat surface clearly shows a plate type (major surface in the plane of the sample's top surface) grain morphology. From this images it can be seen that the size of the plate-type grains was in the range of 5-15 μm. Figures 8(b) and 8(c) show the bright field cross section TEM micrographs of a plane view samples. The grain boundaries in textured BiT are the result of fusing BiT plates together (during high temperature sintering process) mostly with a slight miss-orientation. Fig. 8(c) show a HR-TEM image of the lattice fringes from [001] orientation. Due to the twofold in-plane symmetry, the distinctive stacking of the pseudoperovskite and $(Bi_2O_2)^{2+}$ layers was not observed. Moreover, the layered structure of these materials was found to be useful in decreasing the thermal conductivity due to effective phonon scattering [36].

A3. TERAHERTZ (THz) MEASUREMENTS

The details of the THz spectrometer measurements can be found elsewhere [15]. The spectrometer supports the simultaneous measurements of absorbance and refractive index of solutions over the spectral range from 26.5 GHz to 1.12 THz (0.88 to 37.36 cm^{-1} or 0.268 to 11.3 mm). The signal-to-noise and spectral resolution of this device were significantly high as compared to any previous state-of-the-art instruments. For example, while the dynamic range of a commercial THz time-domain spectrometer is just 10^6 and its spectral resolution is several gigahertz, the dynamic range of the instrument reaches an unprecedented value of 10^{13} and the system achieves a spectral resolution of less than 100 Hz [15, 16, 37-38]. The system provides a coherent radiation source with a power up to 20 mW in the gigahertz-to-terahertz region.

For transmission measurements, we employed a quasi-optical setup. The transmitter module emits THz radiation into free space with a circular horn. The radiation transmitted through the sample is subsequently collected scausing a similar horn and is fed into a receiver module. For temperature dependent measurements, we used a home built temperature controllable setup made of a horizontal solid tube furnace from Thermcraft with 1200 ºC maximum temperature. Temperature of the sample was controlled with an accuracy of ±10 ºC by varying the voltage applied to the tube furnace. The BiT film was placed on a stainless steel sample holder using thermal paste and was attached to an aperture of the tube furnace. An identical aperture and empty sample holder formed reference signals. The translation stage allowed alternative reference and sample measurements under identical conditions. The high dynamic range combined with the ability to detect the phase allowed an accurate measurements of absorption coefficient and refractive index of highly absorptive samples like BiT. The experiment consists of two consecutive measurements for each temperature: (i) Measurements of the reference signals of transmitted intensity and phase shift with an empty sample holder. (ii) Measurements of intensity and phase shift after the BiT sample.

A4. ATOMIC PAIR DISTRIBUTION FUNCTION

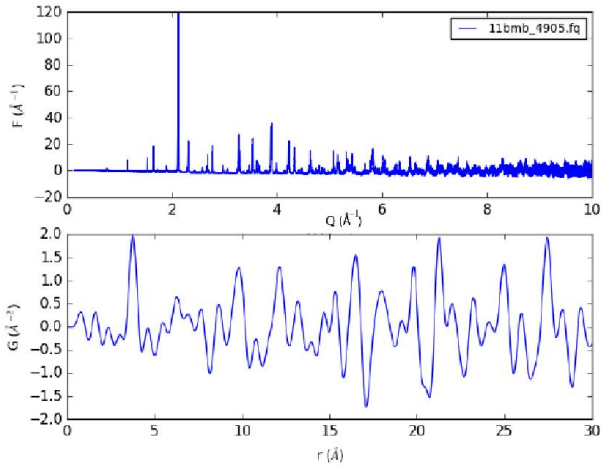

FIG. 9. (Color online) F(Q) and G(r) profiles for BiT from

The atomic pair distribution function analysis can be used to understand local structural changes. PDFgetX was used to compute G(r) from the X-ray diffraction data recorded on $Bi_4Ti_3O_{12}$, as shown in Fig. 9. The $Q_{maxinst}$ was limited to 10 $Å^{-1}$ due to the increased noise. The wavelength used for calculations is 0.414211 Å.

A5. TEMPERATURE DEPENDENT RAMAN SPECTRA

Raman measurements were conducted at the Virginia Tech Vibrational Spectroscopy Laboratory using a Jobin-Yvon HR800 Raman microprobe equipped with a 514 nm laser focused onto the sample through a microscope lens. Machado *et al*.[32] reported two unstable E_u modes in BiT,

one involving the motion of $(Bi_2O_2)^{2+}$ layers in a direction relative to the perovskite blocks and the second one involving the motion of the Bi ions in the perovskite at A site with respect to the TiO_6 perovskite blocks. The unstable E_u mode in layered materials involving movements of $(Bi_2O_2)^{2+}$ layers with respect to the perovskite block, is a general feature of the Aurivillius compounds [32]. These modes occur at very low frequency zone of center optical phonons, in which layers move as rigid units. The remaining unstable mode in BiT has, however, completely different displacement pattern. In order to understand phonon dynamics and the local structural changes with temperature, the temperature dependent Raman spectra (Fig. 10) were

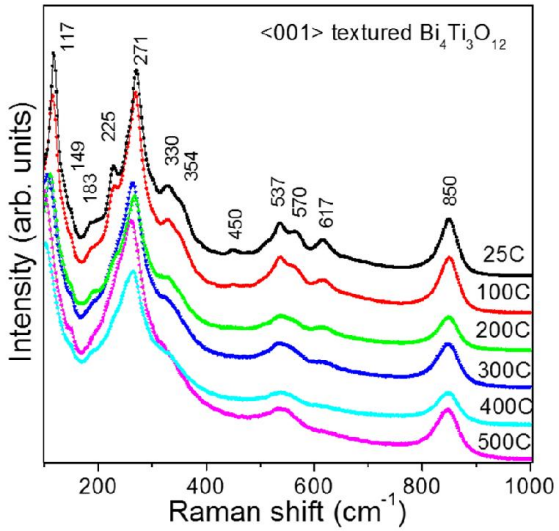

FIG. 10. (Color online) Raman spectra recorded as function of temperature. Change in frequency and intensity of various modes reflects structural changes with respect to the temperature.

recorded.

The heavy Bi ions are expected to exhibit their contribution in the lower frequency regime. The softening of modes at 117 cm^{-1} and 271 cm^{-1} can be treated as a signature that the system undergoes structural transitions. Modes above 200 cm^{-1} stem from TiO_6 octahedra. The Raman modes at 850, 617, 570, 330 cm^{-1} and 450, 354 cm^{-1} are assigned to A_{1g} and B_{1g} modes, respectively. The modes at 537, 271, 225 cm^{-1} are assigned to B_{2g} + B_{3g} modes originating from the lifting of E_g degeneracies. The disappearance and changes in the modes at 617, 570, 450, 330, 225, and 183 cm^{-1} are believed to be due to the reconstructions in overcoming the distortion and octahedral tilting. These changes hint the nanoscale structural changes in the system, which could be the precursors for the structural transformation at the Curie temperature.

A6. UNITCELL VOLUME VERSUS TEMPERATURE

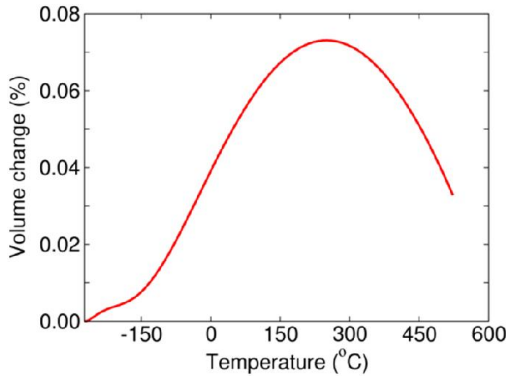

FIG. 11. (Color online) Temperature dependence of the crystallographic volume change for BiT obtained from quasi-harmonic approximation.

REFERENCES

[1] J. Hlinka, T. Ostapchuk, D. Nuzhnyy, J. Petzelt, P. Kuzel, C. Kadlec, P. Vanek, I. Ponomareva, and L. Bellaiche, Physical Review Letters **101**, 167402 (2008).

[2] D. Wang, A. A. Bokov, Z. G. Ye, J. Hlinka, and L. Bellaiche, Nat Commun **7,** 11014 (2016).

[3] M. S. Senn, D. A. Keen, T. C. A. Lucas, J. A. Hriljac, and A. L. Goodwin, Physical Review Letters **116**, 207602 (2016).

[4] D. Nuzhnyy, S. Kamba, P. Kužel, S. Veljko, V. Bovtun, M. Savinov, J. Petzelt, H. Amorín, M. E. V. Costa, A. L. Kholkin, Ph. Boullay, and M. Adamczyk, Phys Rev B **74,** 134105 (2006).

[5] J. M. Perez-Mato, P. Blaha, K. Schwarz, M. Aroyo, D. Orobengoa, I. Etxebarria, and A. García, Phys Rev B **77**, 184104 (2008).

[6] W. S. Choi and H. N. Lee, Phys Rev B **91**, 174101 (2015).

[7] B. H. Park, B. S. Kang, S. D. Bu, T. W. Noh, J. Lee, and W. Jo, Nature **401**, 682 (1999).

[8] C. Chiritescu, D. G. Cahill, N. Nguyen, D. Johnson, A. Bodapati, P. Keblinski, and P. Zschack, Science **315**, 351 (2007).

[9] E. J. Nichols, J. W. J. Shi, A. Huq, S. C. Vogel, and S. T. Misture, J Solid State Chem **197**, 475 (2013).

[10] J. H. Lee, R. H. Shin, and W. Jo, Phys Rev B **84**, 094112 (2011).

[11] A. Shrinagar, A. Garg, R. Prasad, and S. Auluck, Acta Crystallogr A **64**, 368 (2008).

[12] Qingdi Zhou and Brendan J. Kennedy, Chem. Mater. **15,** 4025 (2003).

[13] M. Iwata, K. Ando, M. Maeda, and Y. Ishibashi, Journal of the Physical Society of Japan **82**, 025001 (2013).

[14] M. Kempa, P. Kuzel, S. Kamba, P. Samoukhina, J. Petzelt, A. Garg, and Z. H. Barber, J Phys-Condens Mat **15**, 8095 (2003).

[15] D. K. George, A. Charkhesht, and N. Q. Vinh, Review of Scientific Instruments **86**, 123105 (2015).

[16] N. Q. Vinh, M. S. Sherwin, S. J. Allen, D. K. George, A. J. Rahmani, and K. W. Plaxco, The Journal of Chemical Physics **142**, 164502 (2015).

[17] P. Juhas, T. Davis, C. L. Farrow, and S. J. L. Billinge, Journal of Applied Crystallography **46**, 560 (2013).

[18] Y. Yasuhiro, K. Shinji, and M. Jun'ichiro, Japanese Journal of Applied Physics **45**, 7556 (2006).

[19] A. D. Rae, J. G. Thompson, R. L. Withers, and A. C. Willis, Acta Crystallographica Section B **46**, 474 (1990).

[20] W. Kohn and L. J. Sham, Physical Review **140**, A1133 (1965).

[21] P. Hohenberg and W. Kohn, Physical Review **136**, B864 (1964).

[22] J. P. Perdew, K. Burke, and M. Ernzerhof, Physical Review Letters **77**, 3865 (1996).

[23] P. E. Blöchl, Phys. Rev. B **50**, 17953 (1994).

[24] G. Kresse and D. Joubert, Phys Rev B **59**, 1758 (1999).

[25] G. Kresse and J. Furthmüller, Computational Materials Science **6**, 15 (1996).

[26] G. Kresse and J. Furthmüller, Phys Rev B **54**, 11169 (1996).

[27] J. Min Ku, K. Yong-Il, N. Seung-Hoon, S. Jung Min, J. Chang Hwa, and W. Seong Ihl, Journal of Physics D: Applied Physics **40**, 4647 (2007).

[28] D. J. Singh, S. S. A. Seo, and H. N. Lee, Phys Rev B **82**, 180103 (2010).

[29] A. Shrinagar, A. Garg, R. Prasad and S. Auluck, Acta Cryst. A**64**, 368-375 (2008).

[30] S. Baroni and R. Resta, Phys Rev B **33**, 7017 (1986).

[31] A. Togo and I. Tanaka, Scripta Materialia **108**, 1 (2015).

[32] R. Machado, M. G. Stachiotti, R. L. Migoni, and A. H. Tera, Phys Rev B **70**, 214112 (2004).

[33] See Supplemental Material at [URL will be inserted by publisher] for animated gif files of the phonon modes.

[34] D. Maurya, Y. Zhou, Y. Yan, and S. Priya, Journal of Materials Chemistry C **1**, 2102 (2013)

[35] F. K. Lotgering, J Inorg Nucl Chem **9**, 113 (1959).

[36] C. Chiritescu, D. G. Cahill, N. Nguyen, D. Johnson, A. Bodapati, P. Keblinski, and P. Zschack, Science **315**, 351 (2007).

[37] N. Q. Vinh, S. J. Allen, and K. W. Plaxco, J Am Chem Soc **133**, 8942 (2011).

[38] D. K. George, A. Charkhesht, O. A. Hull, A. Mishra, D. G. S. Capelluto, K. R. Mitchell-Koch, and N. Q. Vinh, J. Phys. Chem. B **120**, 10575 (2016)